Efficient Hydrogen Production at pH 7 in Water with a Heterogeneous Electrocatalyst Based on a Neutral Dimeric Cobalt-dithiolene Complex

Chanjuan Zhang[a], Erwan Prignot[b], Olivier Jeannin[b], Antoine Vacher[b], Diana Dragoe[a], Franck Camerel[a]*, Zakaria Halime[b]*, and Rafael Gramage-Doria[a]*

[a] Université Paris-Saclay, CNRS, Institut de chimie moléculaire et des matériaux d'Orsay, Orsay, France

[b] Univ Rennes, CNRS, ISCR-UMR6226, F-35000 Rennes, France

E-mail : franck.camerel@univ-rennes1.fr; zakaria.halime@universite-paris-saclay.fr; rafael.gramage-doria@univ-rennes1.fr

ABSTRACT: The development of efficient hydrogen production technologies is fundamental for replacing fossil fuel-based energies. As such, electrocatalysts derived from earth abundant metal complexes are appealing, and interesting performances have typically been disclosed under acidic conditions in organic solvents. However, their applicability under relevant pH neutral conditions is underexplored. Herein, we demonstrate that non-ionic, dimeric cobalt-dithiolene complexes supported on multi-wall carbon nanotubes (MWCNTs)/carbon paper (CP) electrode are powerful electrocatalysts for hydrogen production in aqueous media at pH 7. The high turnover numbers encountered (TON up to 50980) after long reaction times (up to 16 hours) are reasoned by the increased electro-active cobalt concentration on the modified electrode, which is *ca.* 4 times higher than that of a state-of-the-art cobalt porphyrin electrocatalyst. These findings point out that immobilizing well-defined, multinuclear low cost metal complexes on carbon material is a promising strategy to design highly electroactive electrodes enabling production of green energies. KEYWORDS: hydrogen, electrocatalysis, cobalt-dithiolene, multi-wall carbon nanotubes, modified-electrode

The use of hydrogen (H_2) as a clean energy carrier to replace fossil fuels is a promising approach in the context of sustainability.[1] It is expected to reduce the carbon footprint in view to help mitigating climate change and minimizing geopolitical issues derived from petrol access. As such the green production of H_2 and O_2 from water, better known as water splitting, is a major research area of interest that have already led to relevant breakthroughs by means of different catalytic technologies.[2] However, there is room for improvement to develop catalysts under mild conditions with high efficiencies.[3]

The overall water splitting transformation is derived from two half reactions namely the ORR (oxygen reduction reaction) and the HER (hydrogen evolution reaction).[4] In the case of the HER, considerable efforts have been devoted to design catalytic systems inspired from the Nature's hydrogenases family, which operate under ambient conditions leading to high levels of hydrogen production.[5] Their active site is constituted by Fe, Ni or Co sites, thereby demonstrating that first-row transition metal species can compete and even outperform catalysts derived from late transition metals.[6] Importantly, the development of catalysts derived from first-row transition metal complexes is highly attractive due to their natural abundance and low toxicity.[7]

In this context, many well-defined coordination complexes based on first row transition metals have been designed and successfully evaluated in the HER.[8] Most of them operate under acidic conditions using organic solvents in order to study their performance as a proof-of-concept.[8] On the other hand, such conditions are rather corrosive and significantly differ from those expected for a practical implementation. Although, electrocatalysts able to reduce protons into H_2 under neutral conditions in water exist, they are mostly based on ionic molecular catalysts[9] or purely heterogeneous systems including nanoparticles and polymers.[10] Herein, we present an approach based on the immobilization of a well-defined, non-ionic dinuclear cobalt complex that turns out to be electrocatalytically active for the production for HER in water at pH 7. The immobilization technique, which relies on sonochemical adsorption of the metal complexes on multi-wall carbon nanotubes (CNTs)/carbon paper (CP) modified-electrode, has already been successfully applied for CO_2 reduction to CO for discrete, monomeric iron-based porphyrins.[11] To the best of our knowledge, this is the first example of a discrete, dinuclear and non-ionic system operating in neutral water for H_2 production.

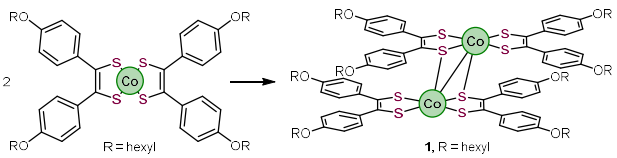

Scheme 1 Molecular structure of the cobalt complex **1**.

Based on previous contributions by Holland and Eisenber dealing with ionic cobalt dithiolene complexes,[12] we anticipated that the dithiolene framework might be an ideal platform for chelating cobalt ions to form a potentially active electrocatalyst for HER. In addition, we reasoned that aliphatic chains located in

the periphery of the cobalt complex may favor its adsorption on carbon nanostructures as well as to prevent its dissolution in polar aqueous electrolytic media.[13] Aliphatic chains were also reported to limit catalyst aggregation on the electrode surface that can obstruct mass transport and inhibit the catalytic activity.[14] Consequently, cobalt complex **1** with hexyl chains was synthesized and isolated as a deep-green solid in a three-step reaction sequence starting from readily available starting materials (Scheme 1, SI).[15] Single crystals of **1** suitable for X-ray analysis were obtained by slow evaporation of a dichloromethane solution (Figure 1).[15] The cobalt complex **1** crystallized into well-defined, dimeric species inside the unit cell, with the inversion center exactly in the middle between the two cobalt atoms. The two cobalt centers form a dimer through two short sulfur-cobalt bonds formed between two monomeric units. In fact, one sulfur atom from one dithiolene ligand forms a bond with the cobalt atom from the other complex, leading to the formation of a cluster-like Co-S-Co-S rectangular motif (Figure 1). Such observation is reminiscent of that observed in the family of the hydrogenase enzymes, in which dithiols (S_2^{2-}) groups are bridging the two active metals, typically [FeFe] and [FeNi].[5] More precisely, the apical S3-Co bond length is 2.3638(8) Å and the Co-Co bond length is 2.7739(5) Å (Figure 1). The sulfur-cobalt distance is shorter than the sum of the van der Walls radius (S: 1.80 Å, Co: 1.25 Å), meaning that an effective Co-S bond is formed within the dimer. The Co-S3 linkages holding the monomeric units together (2.3638(8) Å) are longer than the Co-S bond distances in the CoS2C2 chelate rings (2.15-2.19 Å). Such neutral dimeric motifs with dithiobenzil cobalt-bis(dithiolene) complexes are known but have never been reported with dithiolene ligands carrying long aliphatic carbon chains.[16] In the crystal structure, the dimeric species are stacked along the *a* axis to form columns separated one from another by the carbon chains (Figure S2) and there is no interaction between the central dithiolene complexes in the *bc* plane.[15] The distance between the dimeric cores along the *a* axis is 7.82 Å. The central C-C bond and the C-S bonds on the dithiolene ligands are close (C1-C2 = 1.4057(44) and C3-C4 = 1.3775(43) Å; C1-S1 = 1.7018(31), C2-S2 =1.7061(26), C3-S3 =1.7373(32) and C4-S4 =1.7093(28) Å), indicating that both ligands are in the same oxidation state. These distances, which are intermediate to those observed in the ene-1,2-dithiolate (C-S = 1.75 and C-C = 1.36 Å) and α-dithione forms (C-S = 1.66 and C-C = 1.44 Å), confirm the presence of monoanionic π-radical ligands on the cobalt complex.[17] Thus, the formation of this diamagnetic dimeric complex can be viewed as two antiferromagnetically coupled paramagnetic Co(II) complexes each having two monoanionic π-radical ligands.

Differential scanning calorimetry and polarized optical microscopy analyses have revealed that the dimeric cobalt complex carrying hexyl carbon chains is deprived of mesomorphic properties and only a single melting point was measured at 139.5 °C (Figure S3).[15]

The UV-Vis spectrum of complex **1** in DMF featured a strong absorption at 745 nm (ε = 6590 $L \cdot mol^{-1} \cdot cm^{-1}$) (Figure S4).[15] This absorption band in the near-IR region above 600 nm and can be assigned to a ligand-to-ligand charge transfers from a monoanionic π-radical dithiolene.[18] The presence of S-,S'-coordinated radical monoanions are also readily confirmed in the solid-state IR spectra with the ν(C=S·) stretching frequency at 1112 cm^{-1} (Figure S5).[15,18] Interestingly, the solid-state UV-Vis spectrum recorded on the crystalline compound strongly resemble the one recorded in DMF solution with a broad absorption band centered at 774 nm (Figure S6), suggesting that the apolar dimeric cobalt species remains intact in polar solvent such as DMF. The preservation of the dimeric species in DMF was further confirmed by EPR spectroscopy (Figure S7). The lack of EPR signal is consistent with the presence of a diamagnetic dimeric complex in DMF because the dissociated monomeric species with an odd number of unpaired electrons should have an EPR signal.

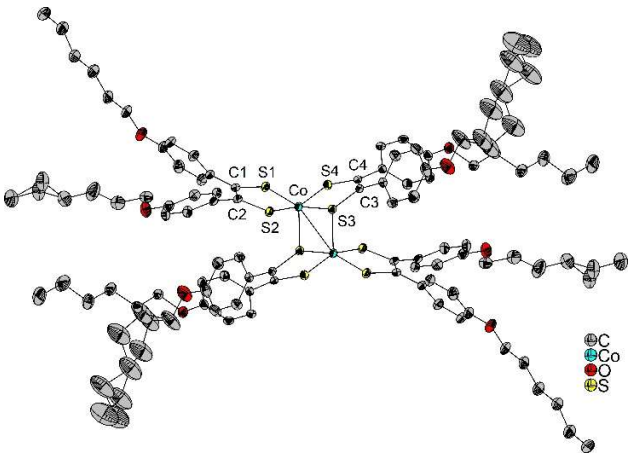

Figure 1 ORTEP view of the cobalt dimer **1** with thermal ellipsoids at 50 % probability and the main atomic numbering scheme (H atoms have been removed for clarity).

The electrochemical behavior of **1** was investigated by cyclic voltammetry (CV) in DMF with 0.1 M $[Bu_4N]PF_6$ as supporting electrolyte (Figure S8).[15] As shown before for other dimeric cobalt dithiolene complexes,[19] complex **1** features three expected one-electron reduction events: one reversible at 0.15 V *vs* NHE corresponding to the reduction of the dimer $\mathbf{1}_2$ to $\mathbf{1}_2^-$ followed by a second irreversible wave at -0.28 V *vs* NHE leading to $\mathbf{1}_2^{2-}$ (in equilibrium with the monomeric species $\mathbf{1}^-$) and a last reversible wave at -0.78 V *vs* NHE corresponding to a one-electron reduction of the monomeric units affording the monomeric $\mathbf{1}^{2-}$. These electrochemical investigations also support the presence of neutral dimeric species in DMF at an open-circuit voltage.

Complex **1** being insoluble in water (due to the presence of long carbon chains) allowed us to study the electrocatalytic HER of the cobalt dimer in an aqueous medium under heterogeneous conditions. The immobilization of the catalyst on the surface of a working electrode as part of a heterogeneous electrochemical cell will thus make it possible to perform such experiments in water as both solvent and proton source. A catalytic ink was first prepared following the typical method by sonicating a mixture containing the cobalt catalyst **1** and MWCNTs in DMF.[11a,20] The CNT-**1** ink was then dropcasted onto the surface of a 10 × 10 mm carbon paper electrode, and the catalytic performances of the modified electrode were evaluated for proton reduction in an electrochemical cell coupled to a Micro GC for the detection and the quantification of the produced gases (Figure S9).[15] For comparison purposes, the catalytic ink CNT-**2** was also prepared from a cobalt(II)-tetraphenylporphyrin (**2**) which is a well-known catalyst for proton reduction and it was used as the reference for this study.[21] Linear sweep voltammetry (LSV) experiments were conducted with pure CNT, CNT-**1** and

CNT-**2** in Ar-saturated 1 M and pH 7 potassium phosphate buffer with a scanning rate of 0.1 V s^{-1} (Figure 2). For potentials below -0.4 V *vs* RHE,[22] CNT-**1** showed an increase of current density that corresponds to water reduction to hydrogen. Notably, CNT-**1** showed a higher current density for water reduction than that of CNT-**2** or pure CNT (Figure 2). The onset potential of water reduction for CNT-**1** was -0.33 V *vs* RHE,[22] which is anodically shifted by 90 mV compare to CNT-**2** (-0.42 V *vs* RHE).[22] To extract the rate-determining step for proton reduction, the Tafel slope has been represented in Figure 3 (Table S1).[15] Rather similar reaction rates are observed for both CNT-**1** and CNT-**2** with Tafel slopes of 177 and 238 mV dec^{-1} respectively.[23] These Tafel slopes were close to the theoretical value of the Volmer step, thereby suggesting that, in contrast with systems operating under a purely homogeneous regime with similar cobalt-dithiolene complexes,[19] a concerted proton-electron transfer (CPET) could be the rate-determining step for the HER catalyzed by CNT-**1** in heterogeneous conditions.[24]

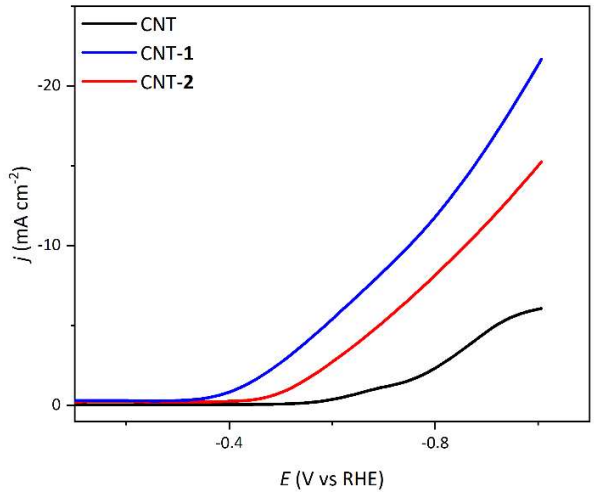

Figure 2 LSV of CNT-**1** (blue), CNT-**2** (red) and pure CNT (black) in Ar-saturated 1 M pH 7 potassium phosphate buffer, scan rate 0.1 V s^{-1}.

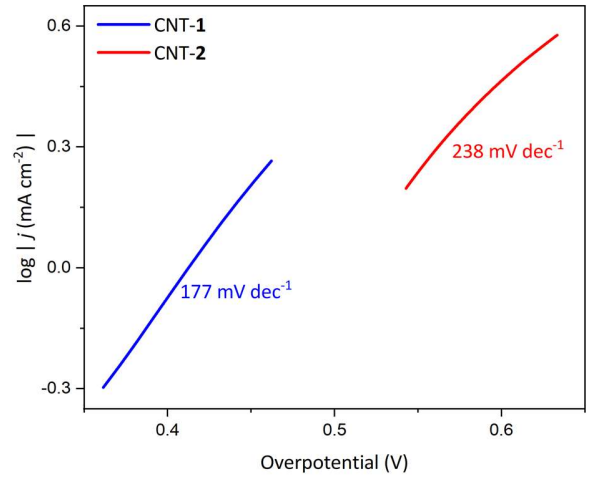

Figure 3 Tafel plots for CNT-**1** (blue) and CNT-**2** (red) in Ar-saturated 1 M pH 7 phosphate buffer, scan rate 0.1 V s^{-1}.

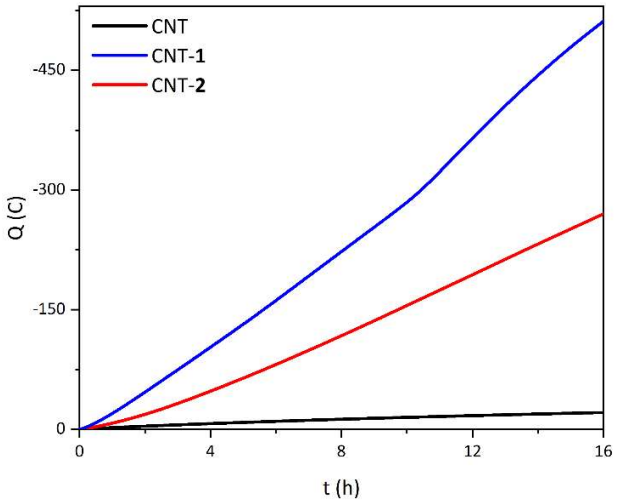

Figure 4 Charge accumulation with controlled potential catalysis of CNT-**1** (blue), CNT-**2** (red) and pure CNT (black) in Ar-saturated 1 M pH 7 phosphate buffer at -0.6 V vs RHE (± 7% error in the measurements).[21] All electrodes had the same deposited cobalt concentration on surface (52 nmol cm^{-2}).

Figure 5 Charge accumulation in a controlled potential catalysis of CNT-**1** (blue) in Ar-saturated 1 M pH 7 phosphate buffer for 16-hours electrolysis (with background) at -0.6 V *vs* RHE, then for 3 times of 4 hour-recycling electrolysis (grey background).

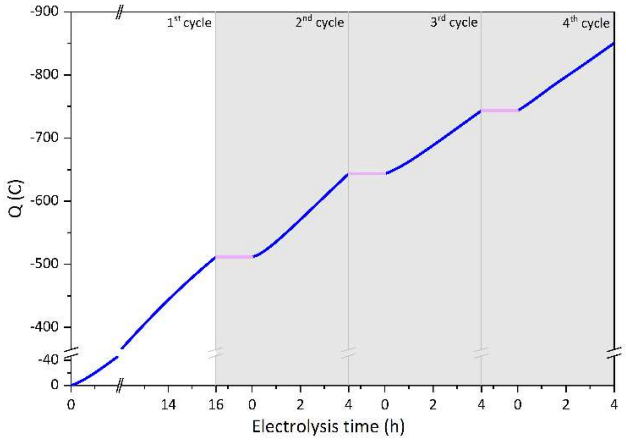

The long-term stabilities and robustness of the catalysts were also investigated over 16 hours at -0.6 V *vs* RHE.[22] All the catalysts show constant increase of the charge accumulation over the time without any sign of fatigue (Figure 4). A control experiment using a modified electrode containing only CNT displayed a significantly low charge accumulation. CNT-**1** exhibited a much better charge accumulation proving that cobalt complex act as a catalyst in the hydrogen production. Importantly, the charge accumulation is much higher with CNT-**1** compared to CNT-**2**, indicating a better catalytic activity. GC gas products analysis results indicated that both CNT-**1** and CNT-**2** featured 100% faradic efficiency for H_2 generation. Additionally, the turnover number (TON) found for CNT-**1** after 16 hours electrolysis was 50980 while CNT-**2** featured a lower value (TON = 26900).[25] Even after the 16-hours electrolysis, the CNT-**1** modified electrode maintains its high activity and selectivity and can be recycled multiple times by just replacing the electrolyte (Figure 5). To further evaluate the stability of our modified electrodes, we also performed galvanostatic electrolysis experiments at a fixed current density (-6.9 mV.cm^{-2}) close

to that observed in the optimized potentiostatic electrolysis experiments (Figure S10). In the case of CNT-**1**, an average observed potential of -0.533 V *vs* RHE can be maintained for more than 10 h. However, as expected from the potentiostatic experiment results, when the same current density is applied to CNT-**2**, a higher average potential of -0.646 V *vs* RHE can be measured. Interestingly, unlike for CNT-**1**, the Co-porphyrin (CNT-**2**) modified electrode shows a sudden decrease in the measured potential after 6 h of electrolysis indicating that the Co-porphyrin based catalyst CNT-**2** is less stable than the CNT-**1** electrode and it likely undergoes significant chemical modifications in these galvanostatic conditions.

The stability of the modified electrode was also evaluated by X-ray photoelectron spectroscopy (XPS) spectra performed on the CNT-**1**/CP electrode before and after electrolysis (Figure 6). The XPS survey displays similar peaks for C 1s, Co 2p, S 2s and S 2p before and after electrolysis indicating that the electrolysis does not induce a major change in the catalyst structure (Figure 6a). The extra peaks appear after electrolysis for K 2s, P 2s and P 2p correspond to the use of the potassium phosphate buffer-based electrolyte. It is worth nothing that a small modification in the high-resolution Co 2p spectrum can be observed after electrolysis (Figure S11). This modification can be attributed to a valence change during the electrolysis indicating the involvement of the Co center in the catalysis. Further evidence for the good stability of the catalyst comes from Fourier-transform infrared spectroscopy (FTIR) analysis, corroborating that the catalyst does not undergo significant structural changes during the electrolysis (Figure 6b).

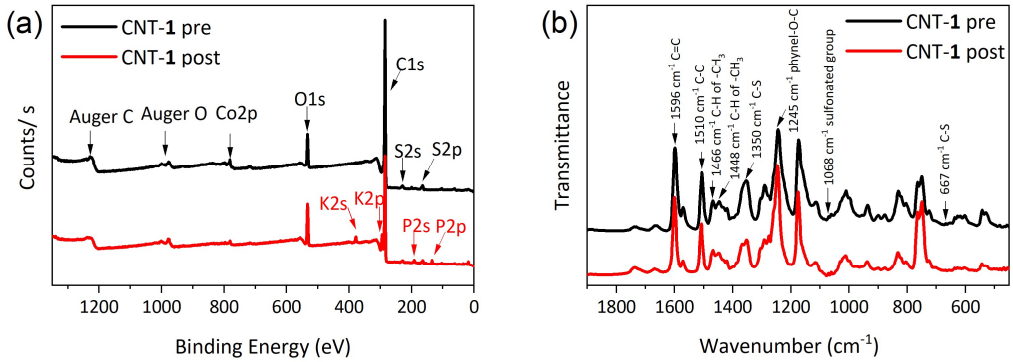

Figure 6 (a) XPS survey, (b) ATR-FTIR spectrum of CNT-**1** before (black) and after electrolysis (red)

Knowing that the working electrode of CNT-**1** and CNT-**2** have the same deposited cobalt metal quantity on surface (52 nmol cm^{-2}), we wondered whether a different electro-ative cobalt metal concentration was responsible for the enhanced activity encountered in CNT-**1** *versus* CNT-**2**. For that, the electroactive cobalt concentration (Γ_{Co}) was calculated by recording the reversible $Co^{II/I}$ redox wave at different scan rate and using the following equation:[26]

$$i_p = \frac{n^2 F^2 v S \Gamma}{4RT}$$

For values below 0.1 V s^{-1}, the catalytic current is dependent on the scan rate and the i_p value shows a linear response with respect to the scan rate. According to the data displayed in Figure 7, on the surface of the working electrodes, the electro-active concentration of CNT-**1** is Γ_{Co} = 12.1 nmol cm^{-2}, corresponding to 23 % of the total amount of Co deposited on the electrode. This value is *ca.* 4 times higher than that corresponding to the electro-active concentration of Co centers in CNT-**2** (Γ_{Co} = 3.4 nmol cm^{-2}, 6.5%). When considering only electro-active Co sites to determine turnover number (eTON), CNT-**2** displays a higher value (eTON = 411 411) than that of CNT-**1** (eTON = 219 087). These results show that even though catalyst CNT-**2** has a higher reaction rate, at the same cobalt centers loading, CNT-**1** based electrode displays a higher hydrogen production (TON = 50980) compared to CNT-**2** modified electrode (TON = 26900). This indicate clearly that the higher hydrogen production in the case of CNT-**1** can be manly attributed to the enhanced active sites accessibility induced by the peripheral aliphatic chains during the immobilization process.

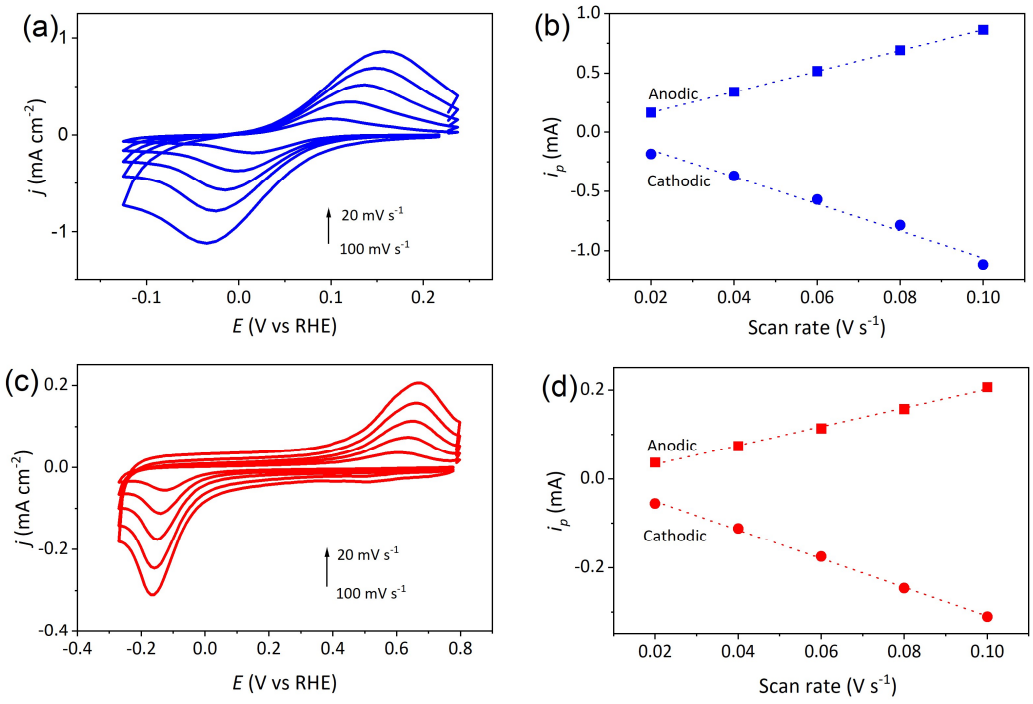

Figure 7 (a) Cyclic voltammetry of CNT-**1** electrode at various scan rate of $Co^{II/I}$ redox wave, (b) i_p vs scan rate, (c) cyclic voltammetry of CNT-**2** electrode at various scan rate of $Co^{II/I}$ wave, (d) i_p *vs* scan rate under Ar in 1 M potassium phosphate buffer, pH 7, $i_p = n^2F^2vS\Gamma/4RT$. $\Gamma_{CNT-1} = 12.1\ nmol\ cm^{-2}$, $\Gamma_{CNT-2} = 3.4\ nmol\ cm^{-2}$

In conclusion, we have reported on the beneficial role of adsorbing a dinuclear cobalt complex into MWCNT/CP electrode for hydrogen evolution under aqueous conditions at pH 7. The electrocatalytic system CNT-**1** features high activity, selectivity and robustness. The cluster-like $[Co_2S_2]$ moiety within **1**, that resembles the active site encountered for Fe and Ni hydrogenases in Nature, together with the peripheral aliphatic chains are responsible for increasing the electro-active cobalt concentration in the electrode which directly translates into enhanced TON values (>50,000) when compared to a benchmark, mononuclear cobalt tetraphenylporphyrin catalyst (**2**). In addition, a single electron transfer to water is identified as the rate-determining step in the case of **1** in stark contrast to systems operating under a purely homogeneous regime with similar cobalt-dithiolene complexes.[19] The present contribution provides fundamentals to further develop sustainable electrodes modified at will for clean energy production.[27] Further research will be devoted to gain insights associated to the reaction mechanism operating for such dinuclear cobalt species.

AUTHOR INFORMATION

Corresponding Author

* Franck Camerel – Univ Rennes, CNRS, ISCR-UMR6226, F-35000 Rennes (France); orcid.org/0000-0003-3380-709X; Email: franck.camerel@univ-rennes1.fr
* Zakaria Halime – Université Paris-Saclay, CNRS, Institut de chimie moléculaire et des matériaux d'Orsay, Orsay (France); orcid.org/0000-0003-3080-9727;
Email: zakaria.halime@universite-paris-saclay.fr
* Rafael Gramage-Doria – Univ Rennes, CNRS, ISCR-UMR6226, F-35000 Rennes (France); orcid.org/0000-0002-0961-4530; Email: rafael.gramage-doria@univ-rennes1.fr

Authors

Chanjuan Zhang – Université Paris-Saclay, CNRS, Institut de chimie moléculaire et des matériaux d'Orsay, Orsay (France)
Erwan Prignot – Univ Rennes, CNRS, ISCR-UMR6226, F-35000 Rennes (France)
Olivier Jeannin – Univ Rennes, CNRS, ISCR-UMR6226, F-35000 Rennes (France)
Antoine Vacher – Univ Rennes, CNRS, ISCR-UMR6226, F-35000 Rennes (France)
Diana Dragoe – Université Paris-Saclay, CNRS, Institut de chimie moléculaire et des matériaux d'Orsay, Orsay (France)

Notes

The authors declare no competing financial interest.

ASSOCIATED CONTENT

The Supporting Information is available free of charge at https://pubs.acs.org/doi/XX.XXX
Full experimental details, synthetic procedures, characterization data, copies of NMR spectra, crystallographic data, and electrochemistry and electrocatalysis data (PDF)

ACKNOWLEDGMENT

E.P., O.J., A.V., F.C. and R.G.-D. acknowledge the CNRS, Université de Rennes 1, Rennes Métropole and Institut des Sciences Chimiques de Rennes ("Projet inter-Equipe") for financial support. C.Z. and Z.H. acknowledge CNRS, CEA Saclay, ICMMO and University Paris-Saclay for the financial support. We thank the China Scholarship Council for supporting C. Zhang (CSC student number 201904910525). We also thank the analytical support facility at ICMMO for their help with XPS analysis.

REFERENCES

(1) Shaner, M. R.; Atwater, H. A.; Lewis, S.; Mcfarland, E. W. A. A comparative technoeconomic analysis of renewable hydrogen production using solar energy. *Energy Environ. Sci.* **2016**, *9*, 2354–2371 .

(2) Wang, M. Y.; Wang, Z.; Gong, X. Z.; Guo, Z. C. The intensification technologies to water electrolysis for hydrogen production – A review. *Renewable Sustainable Energy Rev.* **2014**, *29*, 573–588.

(3) Zhou, Z.; Pei, Z.; Wei, L.; Zhao, S.; Jian, X.; Chen, Y. Electrocatalytic hydrogen evolution under neutral pH conditions: current understandings, recent advances, and future prospects. *Energy Environ. Sci.* **2020**, *13*, 3185−3206.

(4) McCrory, C. C.; Jung, S.; Ferrer, I. M.; Chatman, S. M.; Peters, J. C.; Jaramillo, T. F. Benchmarking hydrogen evolving reaction and oxygen evolving reaction electrocatalysts for solar water splitting devices. *J. Am. Chem. Soc.* **2015**, *137*, 4347−4357.

(5) Vignais, P. M.; Billoud, B.; Meyer. J. Classification and phylogeny of hydrogenases. *FEMS Microbiol. Rev.* **2001**, 25, 455−501.

(6) Eckenhoff, W. T.; McNamara, W. R.; Du, P.; Eisenberg, R. Cobalt complexes as artificial hydrogenases for the reductive side of water splitting. *Biochim. Biophys. Act.* **2013**, 1827, 958–973.

(7) Queyriaux, N.; Jane, R. T.; Massin, J.; Artero, V.; Chavarot-Kerlidou, M. Recent developments in hydrogen evolving molecular cobalt(II)–polypyridyl catalysts. *Coord. Chem. Rev.* **2015**, *304–305*, 3–19.

(8) (a) Felton, G. A. N.; Vannucci, A. K.; Chen, J.; Lockett, L. T.; Okumura, N.; Petro, B. J.; Zakai, U. I.; Evans, D. H.; Glass, R. S.; Lichtenberger, D. L. Hydrogen Generation from Weak Acids: Electrochemical and Computational Studies of a Diiron Hydrogenase Mimic. *J. Am. Chem. Soc.* **2007**, *129*, 12521–12530. (b) Yamaguchi, T.; Masaoka, S.; Sakai, K. Hydrogen Production from Water Catalyzed by an Air-stable Di-iron Complex with a Bio-relevant $Fe_2(\mu\text{-}S)_2$ Core. *Chem. Lett.* **2009**, 38:5, 434-435. (c) Lv, H.; Ruberu, T. P. A.; Fleischauer, V. E.; Brennessel, W. W.; Neidig, M. L.; Eisenberg, R. Catalytic Light-Driven Generation of Hydrogen from Water by Iron Dithiolene Complexes. *J. Am. Chem. Soc.* **2016**, *138*, 11654–11663. (d) Fogeron, T.; Porcher, J. P.; Gomez-Mingot, M.; Todorova, T. K.; Chamoreau, L. M.; Mellot-Draznieks, C.; Li, Y.; Fontecave, M. A cobalt complex with a bioinspired molybdopterin-like ligand: a catalyst for hydrogen evolution. *Dalton Trans.* **2016**, *45*, 14754–14763. (e) Sellmann, D.; Geek, M.; Moll, M. Transition-metal complexes with sulfur ligands. 62. Hydrogen evolution upon reaction of protons with sulfur-coordinated iron(II) complexes. Investigation of the proton, hydrogen and hydride interactions with iron 1,2-benzenedithiolate complexes. *J. Am. Chem. Soc.* **1991**, *113*, 5259–5264. (f) Koshiba, L.; Yamauchi, K.; Sakai, K. Ligand-Based PCET Reduction in a Heteroleptic Ni(bpy)(dithiolene) Electrocatalyst Giving Rise to Higher Metal Basicity Required for Hydrogen Evolution. *ChemElectroChem* **2019**, *6*, 2273–2281. (g) Drosou, M.; Kamatsos, F.; Mitsopoulou, C. A. Recent advances in the mechanisms of the hydrogen evolution reaction by non-innocent sulfur-coordinating metal complexes. *Inorg. Chem. Front.* **2020**, *7*, 37–71.

(9) (a) Stubbert, B. D.; Peters, J. C.; Gray, H. B. Rapid Water Reduction to H_2 Catalyzed by a Cobalt Bis(iminopyridine) Complex. *J. Am. Chem. Soc.* **2011**, *133*, 18070–18073. (b) Wang, J.-W.; Yamauchi, K.; Huang, H.-H; Sun, J.-K; Luo, Z.-M.; Zhong, D.-C.; Lu, T.-B.; Sakai, K. A Molecular Cobalt Hydrogen Evolution Catalyst Showing High Activity and Outstanding Tolerance to CO and O_2. *Angew. Chem. Int. Ed.* **2019**, *58*, 10923–10927.

(10) (a) Xie, X.; Song, M.; Wang, L.; Engelhard, M. H.; Luo, L.; Miller, A.; Zhang, Y.; Du, L.; Pan, H.; Nie, Z.; Chu, Y.; Estevez, L.; Wei, Z.; Liu, H.; Wang, C.; Li, D.; Shao, Y. Electrocatalytic Hydrogen Evolution in Neutral pH Solutions: Dual-Phase Synergy. *ACS Catal.* **2019**, *9*, 8712−8718. (b) Brezinski, W. P.; Karayilan, M.; Clary, K. E.; Pavlopoulos, N. G.; Li, S.; Fu, L.; Matyjaszewski, K.; Evans, D. H.; Glass, R. S.; Lichtenberger, D. L.; Pyun, J. [FeFe]-Hydrogenase Mimetic Metallopolymers with Enhanced Catalytic Activity for Hydrogen Production in Water. *Angew. Chem. Int. Ed.* **2018**, *57*, 11898–11902.

(11) (a) Zhang, C.; Dragoe, D.; Brisset, F.; Boitrel, B.; Lassalle-Kaiser, B.; Leibl, W.; Halime, Z.; Aukauloo, A. Second-sphere hydrogen-bonding enhances heterogeneous electrocatalytic CO_2 to CO reduction by iron porphyrins in water. *Green Chem.* **2021**, *23*, 8979–8987. (b) Zhu, M.; Chen, J.; Huang, L.; Ye, R.; Xu, J.; Han, Y.-F. Covalently Grafting Cobalt Porphyrin onto Carbon Nanotubes for Efficient CO_2 Electroreduction. *Angew. Chem., Int. Ed.* **2019**, *58*, 6595–6599. (c) Maurin, A.; Robert, M. Catalytic CO_2-to-CO conversion in water by covalently functionalized carbon nanotubes with a molecular iron catalyst. *Chem. Commun.* **2016**, *52*, 12084–12087. (d) Tatin, A.; Comminges, C.; Kokoh, B.; Costentin, C.; Robert, M.; Savéant, J.-M. Efficient electrolyzer for CO_2 splitting in neutral water using earth-abundant materials. *Proc. Natl. Acad. Sci. USA* **2016**, *113*, 5526–5529. (e) Aoi, S.; Mase, K.; Ohkubo, K.; Fukuzumi, S. Selective electrochemical reduction of CO_2 to CO with a cobalt chlorin complex adsorbed on multi-walled carbon nanotubes in water. *Chem. Commun.* **2015**, *51*, 10226–10228. (f) Gotico, P.; Halime, Z.; Aukauloo, A. Recent advances in metalloporphyrin-based catalyst design towards carbon dioxide reduction: from bio-inspired second coordination sphere modifications to hierarchical architectures. *Dalton Trans.* **2020**, *49*, 2381–2396.

(12) (a) McNamara, W. R.; Han, Z.; Yin, C.-J.; Brennessel, W. W.; Holland, P. L.; Eisenberg, R. Cobalt-dithiolene complexes for the photocatalytic and electrocatalytic reduction of protons in aqueous solutions. *Proc. Natl. Acad. Sci.* **2012**, *109*, 15594–15599. (b) McNamara, W. R.; Han, Z.; Alperin, P. J.; Brennessel, W. W.; Holland, P. L.; Eisenberg, R. A Cobalt-Dithiolene Complex for the Photocatalytic and Electrocatalytic Reduction of Protons. *J. Am. Chem. Soc.* **2011**, *133*, 15368–15371.

(13) Chen, B.-T.; Morlanés, N.; Adogla, E.; Takanabe, K.; Rodionov, V. O. An Efficient and Stable Hydrophobic Molecular Cobalt Catalyst for Water Electro-oxidation at Neutral pH. *ACS Catal.* **2016**, *6*, 4647−4652.

(14) Choi, J.; Wagner, P.; Gambhir, S.; Jalili, R.; MacFarlane, D. R.; Wallace, G. G.; Officer, D. L. Steric Modification of a Cobalt Phthalocyanine/Graphene Catalyst To Give Enhanced and Stable Electrochemical CO_2 Reduction to CO. *ACS Energy Lett.* **2019**, *4*, 666−672.

(15) See details in the Supporting Information.

(16) (a) Schrauzer, G. N.; Mayweg, V. P.; Finck, H. W.; Heinrich, W. Coordination Compounds with Delocalized Ground States. Bisdithiodiketone Complexes of Iron and Cobalt. *J. Am. Chem. Soc.* **1966**, *88*, 4604−4609. (b) Yu, R.; Arumugam, K.; Manepalli, A.; Tran, Y.; Schmehl, R.; Jacobsen, H.; Donahue, J. P. Reversible, Electrochemically Controlled Binding of Phosphine to Iron and Cobalt Bis(dithiolene) Complexes. *Inorg. Chem.* **2007**, *46*, 5131−5133. (c) Fujiwara, E.; Hosoya, K.; Kobayashi, A.; Tanaka, H.; Tokumoto, M.; Okano, Y.; Fujiwara, H.; Kobayashi, H.; Fujishiro, Y.; Nishibori, E.; Takata, M.; Sakata, M. Conducting Dimerized Cobalt Complexes with Tetrathiafulvalene Dithiolate Ligands. *Inorg. Chem.* **2008**, *47*, 863−874. (d) Jacobsen, H.; Donahue, J. P. Computational Study of Iron Bis(dithiolene) Complexes: Redox Non-Innocent Ligands and Antiferromagnetic Coupling. *Inorg. Chem.* **2008**, *47*, 10037−10045. (e) Enemark, J. H.; Liscomb, W. N. Molecular Structure of the Dimer of Bis(cis-1,2-Bis(Trifluoromethyl)Ethylene-1,2-Dithiolate)Cobalt. *Inorg. Chem.* **1965**, *4*, 1729−1734.

(17) Selby-Karney, T.; Grossie, D. A.; Arumugam, K.; Wright, E.; Chandrasekaran, P. Structural and spectroscopic characteriza-

tion of five coordinate iron and cobalt bis(dithiolene)-trimethylphosphine complexes. *J. Mol. Struct.* **2017**, *1141*, 477−483.
(18) Ray, K.; Bill, E.; Weyhermüller, T.; Wieghardt, K. Redox-Noninnocence of the S,S'-Coordinated Ligands in Bis(benzene-1,2-dithiolato)iron Complexes. *J. Am. Chem. Soc.* **2005**, *127*, 5641−5654.
(19) Letko, C. S.; Panetier, J. A.; Head-Gordon, M.; Tilley, T. D. Mechanism of the Electrocatalytic Reduction of Protons with Diaryldithiolene Cobalt Complexes. *J. Am. Chem. Soc.* **2014**, *136*, 9364−9376.
(20) Abdinejad, M.; Dao, C.; Deng, B.; Sweeney, M. E.; Dielmann, F.; Zhang. X.-A.; Kraatz, H. B. Enhanced Electrochemical Reduction of CO_2 to CO upon Immobilization onto Carbon Nanotubes Using an Iron-Porphyrin Dimer. *ChemistrySelect* **2020**, *5*, 979–984.
(21) Beyene, B. B.; Mane, S. B.; Hung, C. H. Electrochemical hydrogen evolution by cobalt (II) porphyrins: Effects of ligand modification on catalytic activity, efficiency and overpotential. *J. Electrochem. Soc.* **2018**, *165*, H481–H487.
(22) All redox potential are displayed *versus* the reference hydrogen electrode.
(23) Costentin, C.; Savéant, J.-M. Heterogeneous Molecular Catalysis of Electrochemical Reactions: Volcano Plots and Catalytic Tafel Plots. *ACS Appl. Mater. Interfaces* **2017**, *9*, 19894–19899.
(24) Shinagawa, T.; Garcia-Esparza, A. T; Takanabe K. Insight on Tafel slopes from a microkinetic analysis of aqueous electrocatalysis for energy conversion, *Sci. Rep.* **2015**, *5*, 13801 .
(25) TON = mol H_2 produced after 16 hours / mol catalyst deposited.
(26) i_p is the peak current of the $Co^{II/I}$ redox wave, n is the number of electrons, F is faradic constant, S is the geometrical surface area of electrode, v is the scan rate, R is the gas constant and T is the temperature.
(27) Barman, K.; Wang, X.; Jia, R.; Askarova, G.; Hu, G.; Mirkin, M. V. Voltage-Driven Molecular Catalysis of Electrochemical Reactions. *J. Am. Chem. Soc.* **2021**, *143*, 17344−17347.

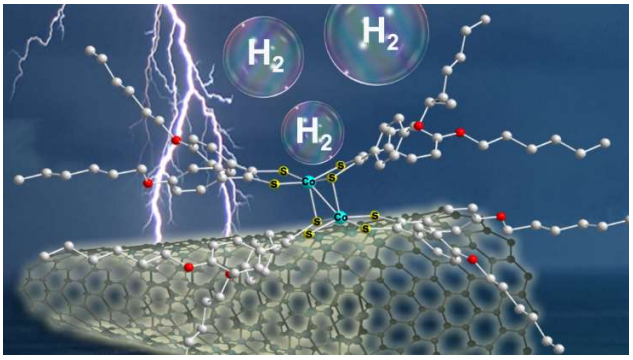

Immobilization of a highly apolar dimeric dithiolene cobalt complexes onto multiwall carbon nanotubes (MWCNTs)/carbon paper (CP) electrodes enables efficient electrocatalytic hydrogen production from water at neutral pH.